Raman Spectroscopy of Boron-Doped Single-Layer Graphene

Yoong Ahm Kim,[†,*] Kazunori Fujisawa,[†] Hiroyuki Muramatsu,[§] Takuya Hayashi,[†] Morinobu Endo,[‡,§] Toshihiko Fujimori,[§] Katsumi Kaneko,[§] Mauricio Terrones,[§,⊥] Jan Behrends,[∥] Axel Eckmann,[¶] Cinzia Casiraghi,[∥,¶] Kostya S. Novoselov,[¶] Riichiro Saito,[#] and Mildred S. Dresselhaus[△]

[†]Faculty of Engineering, [‡]Institute of Carbon Science and Technology, and [§]Research Center for Exotic Nanocarbons (JST), Shinshu University, 4-17-1 Wakasato, Nagano, Japan, [⊥]Department of Physics, Department of Materials Science and Engineering & Materials Research Institute, The Pennsylvania State University, 104 Davey Lab, University Park, Pennsylvania 16802-6300, United States, [∥]Department of Physics, Free University Berlin, Berlin D-14195, Germany, [¶]School of Physics and Astronomy, University of Manchester, Manchester M13 9PL, United Kingdom, [#]Department of Physics, Tohoku University, Sendai 980-8578, Japan, and [△]Department of Electrical Engineering and Computer Science and Department of Physics, Massachusetts Institute of Technology, Cambridge, Massachusetts 02139-4307, United States

ABSTRACT The introduction of foreign atoms, such as nitrogen, into the hexagonal network of an sp^2-hybridized carbon atom monolayer has been demonstrated and constitutes an effective tool for tailoring the intrinsic properties of graphene. Here, we report that boron atoms can be efficiently substituted for carbon in graphene. Single-layer graphene substitutionally doped with boron was prepared by the mechanical exfoliation of boron-doped graphite. X-ray photoelectron spectroscopy demonstrated that the amount of substitutional boron in graphite was ~0.22 atom %. Raman spectroscopy demonstrated that the boron atoms were spaced 4.76 nm apart in single-layer graphene. The 7-fold higher intensity of the D-band when compared to the G-band was explained by the elastically scattered photoexcited electrons by boron atoms before emitting a phonon. The frequency of the G-band in single-layer substitutionally boron-doped graphene was unchanged, which could be explained by the p-type boron doping (stiffening) counteracting the tensile strain effect of the larger carbon–boron bond length (softening). Boron-doped graphene appears to be a useful tool for engineering the physical and chemical properties of graphene.

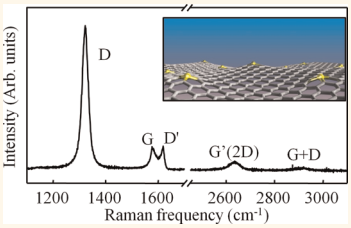

KEYWORDS: graphene · boron · substitution · Raman

Graphene consists of a monolayer network of sp^2-hybridized carbon atoms.[1−3] This unique 2-D structure results in unique properties, such as a high carrier mobility,[4,5] a high Young's modulus, a high thermal conductivity,[6,7] and a low optical absorbance.[8,9] All of these properties make graphene a material which could be used in the fabrication of electronic devices,[10−12] supercapacitors,[13,14] batteries,[15,16] solar cells,[17] sensors,[18,19] and polymer composites.[20,21]

Chemical doping by ion implantation is the common way to dope semiconductors. Impurities are introduced in the crystal lattice as substitutional atoms. For graphene, boron and nitrogen are the best candidates that could be used to substitute for carbon atoms since both elements are carbon's neighbors in the periodic table; that is, they have three and five electrons in their outer shells, respectively. Nitrogen atoms have been explored as an effective dopant for graphene.[22−26] Boron has one fewer valence electron when compared to carbon, and therefore, it is expected to induce p-type doping. Substitutional doping also has significant effects on the graphene structure; that is, it introduces chemical disorder since the B−C bond is 0.5% longer than the C−C bond.[27]

It is noteworthy that boron doping has been successfully used to modify the electronic, mechanical, and oxidative properties of graphite and carbon nanotubes.[28−32] The maximum reported solubility of boron in graphite has been 2.35% at 2350 °C.[28] The substitutional boron atoms induced a perturbed flat geometry, and the modified electronic structure of the graphite plane was verified by scanning tunneling microscopy.[29] In addition, boron is used as an effective coating agent for carbon−carbon composites for engineering applications,[30] and boron-doped carbons are used as high-performance anode materials in lithium ion batteries.[31] Scanning tunneling microscopy has demonstrated that boron-doped multiwalled carbon nanotubes exhibit a semimetallic character with vanishing or narrow band gaps.[32,33]

Boron-doped graphene is of fundamental interest because recent calculations have shown that a sufficiently high boron concentration gives rise to quantum interference effects without affecting the outstanding transport properties of graphene.[34] Furthermore, it has been shown that, in nanoribbons, the bonding of boron at the edges can

* Address correspondence to yak@endomoribu.shinshu-u.ac.jp.

Received for review April 19, 2012 and accepted June 7, 2012.

Published online June 07, 2012
10.1021/nn301728j

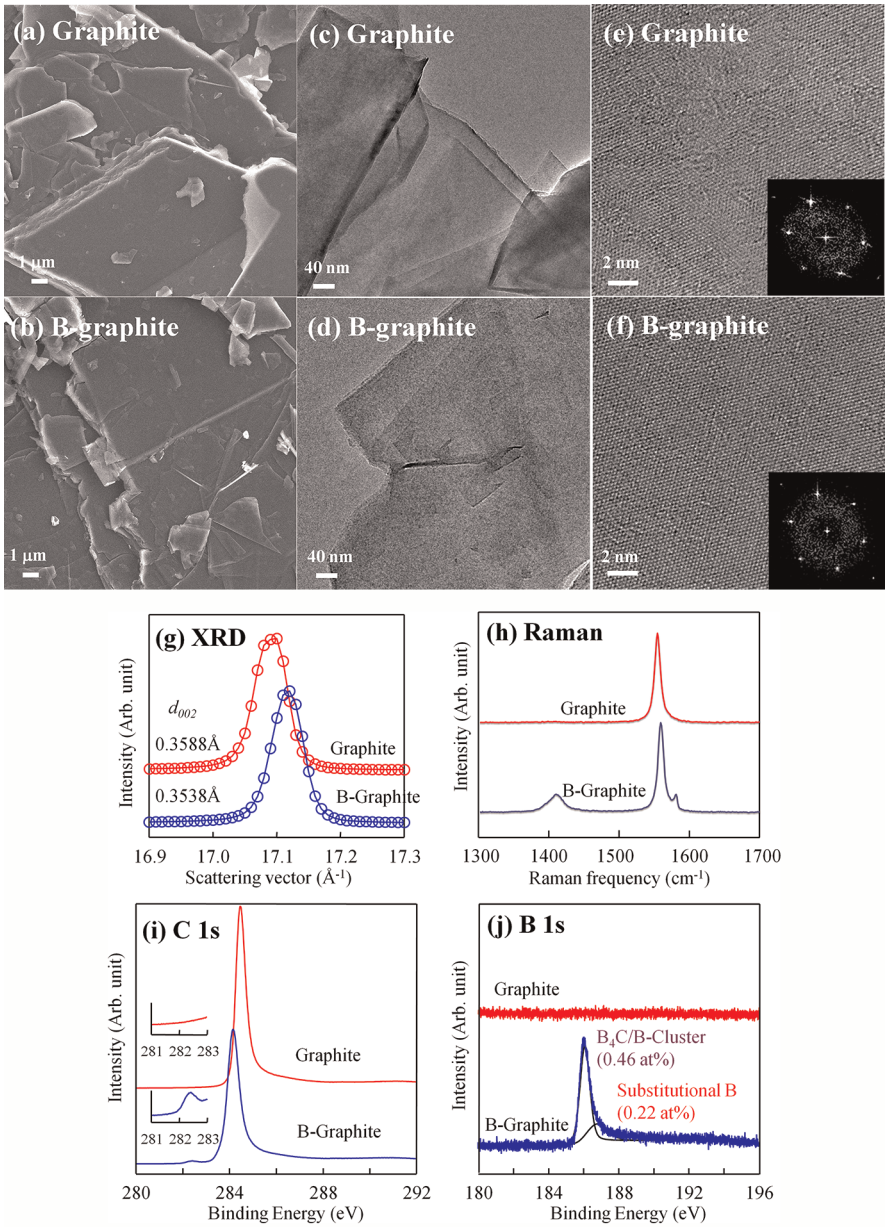

Figure 1. (a–f) Typical SEM, TEM, and atomic-scale TEM images of the pure and boron-doped graphite. (g) X-ray diffraction and (h) Raman spectra, (i) the C1s and (j) the B1s XPS spectra of pure and boron-doped graphite. There is no difference between pristine and boron-doped graphite in the SEM and TEM images.

induce a transition from metallic to semiconducting behaviors.[35] To the best of our knowledge, this is the first Raman study on boron-doped single-layer graphene: previous works have only discussed boron doping in graphite[36–38] and few-layered graphene.[39] In the first case, ion implantation was used, whereas in the second case, the samples were produced by arc-discharge in the presence of gases.

In the present study, we prepared single-layer graphene substitutionally doped with boron *via* the mechanical exfoliation of boron-doped graphite. The boron-doped graphite was prepared by thermally treating graphite with a boron compound at 2450 °C using a graphite furnace. The aim of this work is to investigate how substitutional doping and chemical disorder change the properties of graphene.

RESULTS AND DISCUSSION

Single-crystal graphite (Kish graphite), prepared by precipitation from molten iron, was used as a host material for boron doping.[40] The graphite was several nanometers thick and exhibited a rectangular plate-like morphology and a flat surface with a metallic luster (Figure 1a). A transmission electron microscope (TEM) image showed that the Kish graphite consisted of stacked thin layers and had a predominantly rectangular edge structure (Figure 1c). There was no change in the macro- and nanotexture of graphite, even after

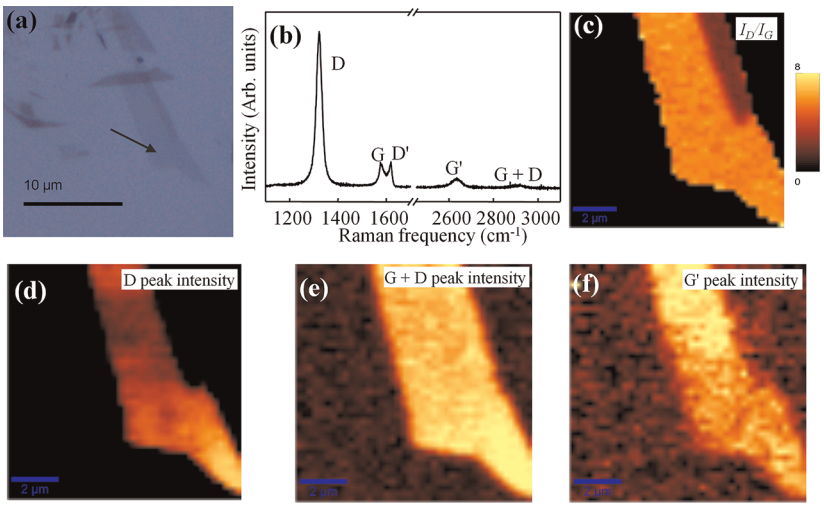

Figure 2. (a) Optical microscope image of the boron-doped single-layer graphene (indicated by the arrow) on an SiO_2/Si substrate; (b) Raman spectrum obtained using a 633 nm laser line, and spatial maps of (c) I_D/I_G, the intensities of the (d) D-band, (e) G + D-band, and (f) G′-band. The integrated intensity of the D-band is 7-fold that of the G-band.

the boron doping at high temperatures (Figure 1b,d). High-resolution TEM (HRTEM) images of both samples did not reveal any distinctive differences between the pristine and boron-doped graphite (Figure 1e,f). However, boron doping induced a subtle change in the crystallographic structure, which was verified by the decrease in the interlayer spacing of the graphite (002) diffraction line (Figure 1g) and the higher intensity D-band (defect-induced mode) in the Raman spectra (Figure 1h).[41] X-ray photoelectron spectroscopy (XPS) was used to confirm the presence of the boron atoms that were introduced *via* the high-temperature thermal treatment of graphite (Figure 1i,j). The strong C1s spectra peak located at 284.4 eV was assigned to the sp^2-bonded carbon atoms, and the small B1s spectral feature at 282.2 eV corresponds to the presence of boron atoms in graphite.[42] A subtle downshift in the binding energy and a slight increase in the full width at half-maximum (fwhm) intensity were detected in the C1s peak of the boron-doped graphite. The change in binding energy could be explained through the lowering of the Fermi level by the formation of a chemical bond between carbon and electron-deficient boron. The increase in the fwhm is attributable to the increase in structural disorder due to the longer boron−carbon bonds. The new peak observed at 282.2 eV (insets in Figure 1i) comes from the carbidic boron−carbon bond compound; this also confirms the presence of boron atoms in graphite.[42] In addition, the presence of the substitutional boron atoms in graphite was verified again by a close observation of the B1s region in the spectrum (Figure 1j). The strong peak located *ca.* 186.5 eV was assigned to a boron cluster and boron carbide, whereas the broad and weak peak at *ca.* 187.0 eV originated from the substitutional boron atoms within graphite.[42] These results showed that the amount of substitutional boron in graphite from the total boron concentration (0.69 atom %), calculated *via* the curve fitted areas for their corresponding spectra, was 0.22 atom %. In addition, the diamagnetic susceptibility of boron-doped graphite was -1.66×10^{-6} emu/g at room temperature, which is around 1/5 of the value expected for pristine graphene. The substitutional boron atoms act as electron acceptors, which lower the Fermi level, and decrease the diamagnetic susceptibility. This observation also supports the presence of boron atoms at trigonal sites.

Micromechanical exfoliation of boron-doped graphite with adhesive tape was used to obtain high-quality boron-doped single-layer graphene. The exfoliation was performed by the repeated folding and unfolding of the tape, which was attached to boron-doped graphite, and the flakes were transferred to a SiO_2/Si substrate. Optical microscope images show graphene flakes of atomic and micrometer thickness (Figure 2a). The Raman maps were measured using a 633 nm laser line on optically transparent, large single-layer graphene (as indicated by the arrow in Figure 2a). Raman maps constitute an efficient method for studying the effect of the number of layers and defects in graphene.[43,44] The boron-doped graphene exhibited two bands characteristic of graphene: the G-band at 1580 cm^{-1} corresponding to the stretching vibration of the carbon−carbon bond, and the G′-band at 2725 cm^{-1} due to a second-order two-phonon process, activated by double resonance processes.[45,46] In addition, three new bands appeared at 1345, 1622, and 2950 cm^{-1},[45,46] which were attributed to the defect-induced double resonance Raman feature (the D- and D′-bands) and the combination of G + D (the combination of phonons with different momentum around the Γ and K points). The intensity of the D-band was 7 times greater than that of the G-band, and the peak intensity of the D′-band was equal to that of the G-band (Figure 2b).

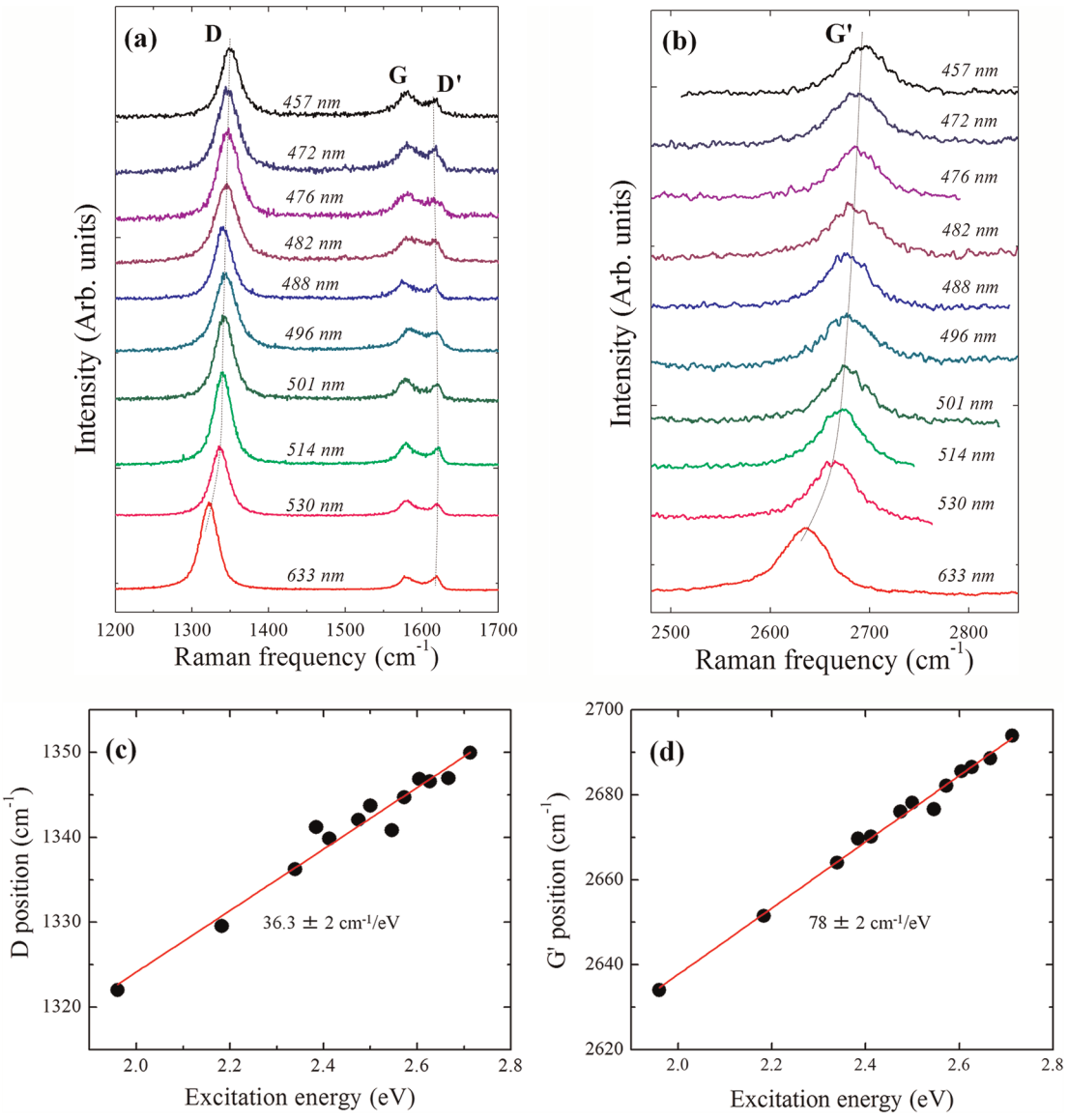

Figure 3. (a) First-order and (b) second-order resonant Raman spectra of boron-doped single-layer graphene using laser lines from 457 to 633 nm. The laser excitation energy dependency of the (c) D-band and (d) G′-band frequencies.

The low intensity of the D-band in boron-doped graphite (Figure 1h) indicates a strong interaction between the boron and carbon atoms in different layers. More specifically, the scattering amplitude of a photoexcited electron by a boron atom in bilayer graphene is expected to be a half of the value for single graphene because the electronic structure of AB-stacked bilayer graphene is either a symmetric or an antisymmetric combination of wave functions of π electrons in the two layers. For multiple layers, since the wave function consists of the wave functions for various layers, the scattered amplitude becomes inversely proportional to the number of layers. These two bands (*e.g.*, the D- and D′-bands) are closely associated with the density of defects in graphene.[47,48] However, in order to ensure structural integrity, the number of defects should be kept to a minimum because the sample was prepared by thermally treating the graphite with a boron compound at 2450 °C. Thus, the strong defect-induced peaks (the D- and D′-bands) originate by chemical disorder from the substitutional boron atoms embedded within the graphene. The Raman features of the boron-doped graphene are similar to those of the defective graphene prepared by ion bombardment, at 10^{13} Ar^{+}/cm^{2}.[47,48] Assuming the substitutional boron atoms to be equivalent to vacancy-like defects, the following empirical equation was used to measure the defect density in ion-bombarded graphene: $I_D/I_G = 102/L_D^2$, where I_D/I_G is the intensity of the G-band divided by the intensity of the D-band and L_D indicates the density of defects in graphene.[47] The calculated average boron−boron distance (L_D) in boron-doped single-layer graphene within the laser spot size was ~4.76 nm. The boron atoms were predicted to be

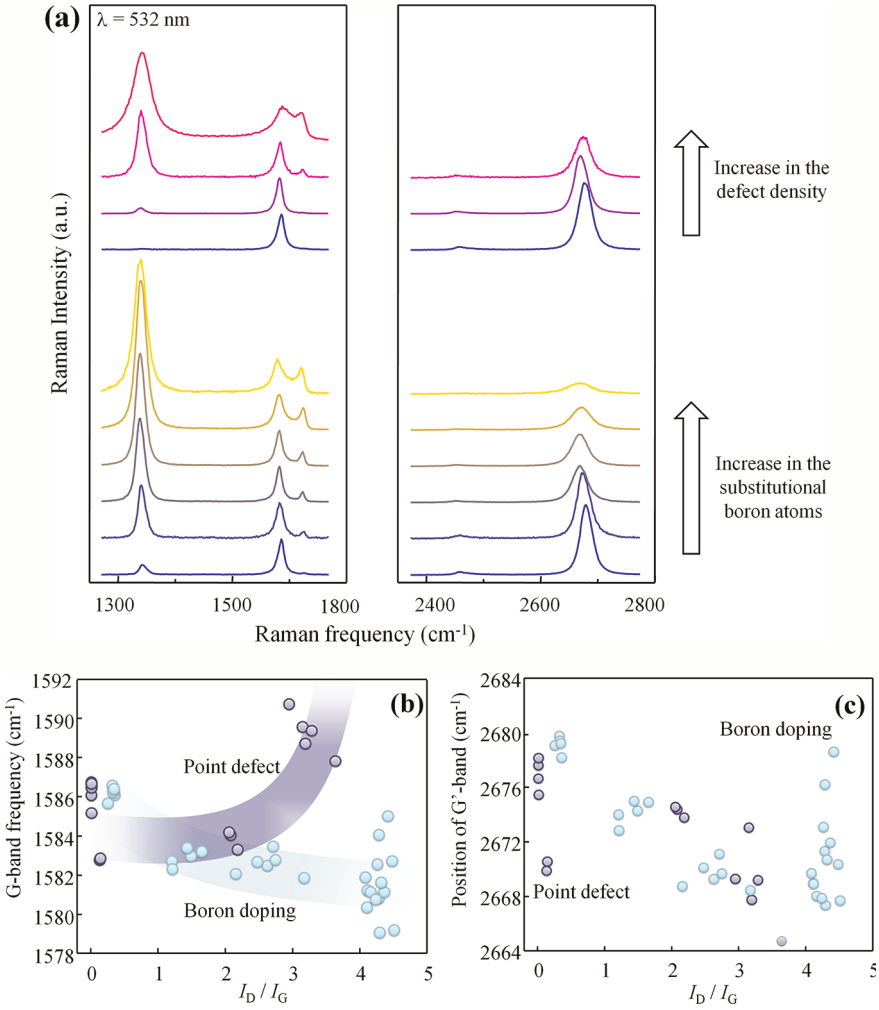

Figure 4. (a) Raman spectra of single-layer graphene samples with different amounts of boron doping, using a 532 nm laser line. The relationships between the G-band position (b) and the G′-band position (c) and I_D/I_G. The Raman spectra of the defective graphene prepared by argon plasma are shown for comparison in (a) by the dark circled points given in (b) and (c).

substituted into the sp^2-carbon hexagonal network with an average boron−boron distance of 4.76 nm, in order to relieve the strain generated by the longer boron−carbon bond. In other words, the substitutional boron atoms can induce a breaking of the translational symmetry of the sp^2 hexagonal carbon network, thereby resulting in the evolution of the D-band intensity caused by both electron-defect elastic scattering and electron−phonon inelastic scattering.[49] The calculated average boron−boron distance of ~4.76 nm within graphene corresponds to the scattering length for elastic scattering. According to Jiang's theoretical studies,[50,51] a typical lifetime for emitting a phonon is 1 ps (for the LO G-band in graphite) and 0.65 ps (for the LO G-band in a (10,10) nanotube) for a photoexcited electron with energy less than 2.5 eV. If we multiply the Fermi velocity of graphene (10^6 m/s), a mean free path for a photoexcited electron to emit a phonon is 650 nm. If we adopted a time of 0.03 ps for emitting any phonon among the LA or TA or LO or TO phonon modes, a mean free path for emitting any of these phonons should be on order of 30 nm. This means that the photoexcited electron is scattered elastically by boron atoms before emitting a phonon. Thus, we believe that the large intensity of the D-band in boron-doped single-layer graphene could be explained by the electron−boron elastic scattering process.

Raman maps of a boron-doped single-layer graphene were recorded to confirm this prediction (Figure 2c−f). The relatively homogeneous spatial image of I_D/I_G (the integrated intensity of the D-band divided by the integrated intensity of the G-band) (Figure 2c) indicates the homogeneous incorporation of boron atoms into trigonal sites of graphene. Figure 2d−f shows spatial images of the intensity of the D-band, the G + D-band, and the G′-band, respectively, which verify the presence of boron atoms across graphene. The undulation in the brightness of each map comes from the step used to get the Raman map (*ca.* 200 nm) (The laser spot size is −500 nm).

The vibrational properties of the boron-doped single-layer graphene were further investigated using

different laser lines between 457 and 633 nm (Figure 3a,b). The G-band frequencies do not depend on the excitation laser energy because it is a Raman-active first-order mode, whereas the peak frequency of the D-band and the G′-band features increases with increasing laser excitation energy. Such a dispersive behavior was well explained by a double resonance process.[45,46] The D′-band located at 1620 cm^{-1} showed a weak dispersive behavior. The excitation laser energy dependence of the frequencies of the D-band (Figure 3c) and the G′-band (Figure 3d) was plotted for the boron-doped single-layer graphene. Both figures were fitted using straight lines. The slope from the D-band was 37.4 cm^{-1}/eV, which was about half that of the slope from the G′-band (76.7 cm^{-1}/eV). The strong dispersive behavior of the G′-band occurs because it is a second-order process related to a phonon near the K point in graphene. Such a low value of the D-peak dispersion slope, as revealed by theoretical calculation of the Raman D-peak dispersion as a function of doping,[52] supports the hole-doped graphene by the substitutional boron doping.

Raman studies were carried out on several graphene samples with different amounts of substitutional boron atoms (Figure 4a). The Raman spectra of defective graphene prepared by an argon plasma[47,48] are shown for comparison in Figure 4a. The upshifted G-band position in the argon plasma applied graphene can be explained by the formation of point-like defects. However, for our boron-doped single-layer graphene, there was no distinctive upshift in the G-band position, even though the G-band is upshifted for both hole and electron doping.[53] In addition, a consecutive increase in the intensity of the D- (1350 cm^{-1}) and D′-bands (1620 cm^{-1}) and a continuous decrease in the intensity of the G′-band were observed as the amount of substitutional boron atoms (defect density) increased. The extremely low intensity of the G′-band and the asymmetric shape of the G-band suggest the saturation of substitutional boron doping in the graphene layer.[54] However, when the relationship between the G-band position and I_D/I_G was plotted (Figure 4b), a substantial difference in the G-band position for the defective ion-implanted and the boron-doped graphene was apparent. The constant G-band position for the single-layer graphene with different amounts of boron could be explained by the stiffening caused by p-type doping[45] counteracting the softening caused by the boron-induced tensile strain.[55,56] If the origin of the downshift is due to changes of the tensile strain, the downshift of the G′-band (the same C−C bond stretching vibration) would be slightly smaller than twice the downshift of the G-band. Thus, we compared the G′-band position as a function of I_D/I_G for both boron-doped and argon-implanted single-layer graphene samples (see Figure 4c). The continuous downshift of the G′-band position for boron-doped single-layer graphene is clearly observed when the value of I_D/I_G increases up to 3. The slope of the downshift is 4 $cm^{-1}/(I_D/I_G)$ for the G′-band, which is twice the value of 2 $cm^{-1}/(I_D/I_G)$ for the G-band. However, for $I_D/I_G = 4$ or higher, a large variation of the G′-band position appears. In this case, a simple model based on the change of the spring constant for the vibration does not work anymore because, for such larger amounts of doping, the electronic structure is modified by strain, and the double resonance conditions for the phonon q vectors could be modified.

CONCLUSIONS

We report the preparation of boron-doped single-layer graphene by the mechanical exfoliation of boron-doped graphite. The boron-doped graphite was prepared by thermally treating graphite with a boron compound at 2450 °C in a graphite furnace. The amount of substitutional boron atoms in a single crystal of graphite was ∼0.22 atom %, based on the curve fitted areas of their corresponding peaks from XPS measurements. The introduction of substitutional boron atoms into a single graphene sheet was verified by the 7-fold increase in the intensity of the D-band and the equal intensity of the D′-band and the G-band. In addition, the Raman maps of the defect-induced bands confirmed the presence of boron atoms across the graphene sheet. The Raman spectra reveal that the boron atoms were on average spaced 4.76 nm apart in the graphene layer.

Boron atoms have great potential as an efficient doping agent for engineering the physical and the chemical properties of graphene, and the corresponding properties of boron-doped graphene should be thoroughly investigated. Substitutionally introduced boron atoms induce a large change in the coupling interaction between the graphene layers; therefore, the optical and transport properties of boron-doped graphene should be investigated as a function of the number of layers. In addition, the optical and transport properties of free-standing boron-doped single-layer graphene must also be determined in order to exclude the effect of the SiO_2/Si substrate. The introduction of boron also increases the number of hole-type charge carriers, which enhances the conductivity. If the amount of boron could be increased to 4−5 atom %, it is predicted that heavily boron-doped graphene would likely be a superconductor.[57] The decrease in the electron density of the substitutional boron atoms is accompanied by an increase in the electron density on nearby active carbon sites. Thus, the chemical and electrochemical activity of the boron-doped graphene, such as the oxygen reduction reaction, should be evaluated. The combined effects of substitutional nitrogen or phosphorus and boron atoms in graphene should also be explored. Experimental methods for distinguishing between single and double layers in the boron-doped graphene and for controlling the

amount of substitutional boron atoms in graphene must also be developed. STM and TEM characterization could also be used to visualize substitutional single boron atoms in graphene. Highly conductive boron-doped graphene could be used as a multifunctional filler in composites and electrode materials in energy storage devices and in transparent conductive films. Heavily boron-doped graphene may be used as a superconductor, and boron atoms could be used to modify the edges of graphene nanoribbons.

EXPERIMENTAL SECTION

The single-crystal Kish graphite used in this study was provided by the Pohang Iron and Steel Company (POSCO, Korea), and boric acid (H_3BO_3) (Wako Company, Japan) was used as the dopant. The boron doping process was achieved by mixing 5 wt % boric acid with graphite and thermally treating the mixture at 2450 °C for 30 min using a graphite furnace in an argon atmosphere. The atomic resolution transmission electron microscopy (HR-TEM) images of graphene before and after boron doping were obtained using a double C_S correction (CEOS GmbH) equipped microscope (JEM-2100F, 80 kV, JEOL, Japan). The doping type and the amount of boron in the graphite were evaluated using X-ray photoelectron spectroscopy (XPS, AXIS-ULTRA DLD, Kratos Analytical) with an monochromatized Al Kα X-ray source with a 15 mA emission current and a 15 kV accelerating voltage. The powder diffraction patterns of graphite before and after boron doping were obtained using synchrotron X-ray diffraction (SPring-8 BL02B2). The sample for Raman study was fabricated using a simple mechanical exfoliation procedure described in ref 1. The Raman spectra of graphene on SiO_2/Si were measured with different spectrometers: a Witec confocal Raman spectrometer, equipped with an excitation line of 633 nm and 100× objective, was used to perform Raman mapping. A triple monochromator Dilor XY Raman spectrometer, equipped with an Ar−Kr ion laser and 100× objective, was used to perform multiwavelength Raman spectroscopy. In both cases, the laser power was kept well below 1 mW to avoid damage of the sample and heating effects. Further measurements were taken with a Renishaw InVia Raman spectrometer equipped with a 532 nm laser line and 100× objective.

Conflict of Interest: The authors declare no competing financial interest.

Acknowledgment. We acknowledge support from the Research Center for Exotic NanoCarbon Project, Japan Regional Innovation Strategy Program by the Excellence, JST. Y.A.K. and R.S. acknowledge, respectively, MEXT grant (Nos. 24310088 and 20241023). M.S.D. acknowledges support from NSF-DMR-10-04147. C.C. acknowledges the Humboldt Foundation for financial support, S. Reich for access to the Dilor XY spectrometer, P. Klar and T. Georgiou for assistance with the samples. The synchrotron radiation experiments were performed at the BL02B2 of Spring-8 with the approval of the Japan Synchrotron Radiation Research Institute (JASRI) (Proposal No. 2010B1485).

Note Added after ASAP Publication. After this paper was published on the Web June 13, 2012, a correction was made to the TOC graphic and abstract graphic. The corrected version was reposted June 18, 2012.

REFERENCES AND NOTES

1. Novoselov, K. S.; Geim, A. K.; Morozov, S. V.; Jiang, D.; Zhang, Y.; Dubonos, S. V.; Grigorieva, I. V.; Firsov, A. A. Electric Field Effect in Atomically Thin Carbon Films. *Science* **2004**, *306*, 666–669.
2. Novoselov, K. S.; Geim, A. K.; Morozov, S. V.; Jiang, D.; Katsnelson, M. I.; Grigorieva, I. V.; Dubonos, S. V.; Firsov, A. A. Two-Dimensional Gas of Massless Dirac Fermions in Graphene. *Nature* **2005**, *438*, 197–200.
3. Geim, A. K.; Novoselov, K. S. The Rise of Graphene. *Nat. Mater.* **2007**, *6*, 183–191.
4. Bolotin, K. I.; Sikes, K. J.; Jiang, Z.; Klima, M.; Fudenberg, G.; Hone, J.; Kim, P.; Stormer, H. L. Ultrahigh Electron Mobility in Suspended Graphene. *Solid State Commun.* **2008**, *146*, 351–355.
5. Zhang, Y.; Tan, Y. W.; Stormer, H. L.; Kim, P. Experimental Observation of the Quantum Hall Effect and Berry's Phase in Graphene. *Nature* **2005**, *438*, 201–204.
6. Lee, C.; Wei, X.; Kysar, J. W.; Hone, J. Measurement of the Elastic Properties and Intrinsic Strength of Monolayer Graphene. *Science* **2008**, *321*, 385–388.
7. Balandin, A. A.; Ghosh, S.; Bao, W. Z.; Calizo, I.; Teweldebrhan, D.; Miao, F.; Lau, C. N. Superior Thermal Conductivity of Single-Layer Graphene. *Nano Lett.* **2008**, *8*, 902–907.
8. Sheehy, D. E.; Schmallan, J. Optical Transparency of Graphene As Determined by the Fine-Structure Constant. *Phys. Rev. B* **2009**, *80*, 193411.
9. Nair, R. R.; Blake, P.; Grigorenko, A. N.; Novoselov, K. S.; Booth, T. J.; Stauber, T.; Peres, N. M. P.; Geim, A. K. Fine Structure Constant Defines Visual Transparency of Graphene. *Science* **2008**, *320*, 1308.
10. Prasher, R. Graphene Spreads the Heat. *Science* **2010**, *328*, 185–186.
11. Sordan, R.; Traversi, F.; Russo, V. Logic Gates with a Single Graphene Transistor. *Appl. Phys. Lett.* **2009**, *94*, 073305.
12. Lin, Y.; Dimitrakopoulos, C.; Jenkins, K. A.; Farmer, D. B.; Chiu, H.; Grill, A.; Avouris, P. 100-GHz Transistors from Wafer-Scale Epitaxial Graphene. *Science* **2010**, *327*, 662.
13. Liu, C.; Yu, Z.; Neff, D.; Zhamu, A.; Jang, B. Z. Graphene-Based Supercapacitor with an Ultrahigh Energy Density. *Nano Lett.* **2010**, *10*, 4863–4868.
14. Zhu, Y.; Murali, S.; Stoller, M. D.; Ganesh, K. J.; Cai, W.; Ferreira, P. J.; Pirkle, A.; Wallace, R. M.; Cychosz, K. A.; Thommes, M.; *et al.* Carbon-Based Supercapacitors Produced by Activation of Graphene. *Science* **2011**, *332*, 1537–1541.
15. Yoo, E.; Kim, J.; Hosono, E.; Zhou, H.-S.; Kudo, T.; Honma, I. Large Reversible Li Storage of Graphene Nanosheet Families for Use in Rechargeable Lithium Ion Batteries. *Nano Lett.* **2008**, *8*, 2277–2282.
16. Wang, H.; Yang, Y.; Liang, Y.; Robinson, J. T.; Li, Y.; Jackson, A.; Cui, Y.; Dai, H. Graphene-Wrapped Sulfur Particles as a Rechargeable Lithium−Sulfur Battery Cathode Material with High Capacity and Cycling Stability. *Nano Lett.* **2011**, *11*, 2644–2647.
17. Wang, X.; Zhi, L.; Müllen, K. Transparent, Conductive Graphene Electrodes for Dye-Sensitized Solar Cells. *Nano Lett.* **2008**, *8*, 323–327.
18. Shan, C. S.; Yang, H. F.; Han, D. X.; Zhang, Q. X.; Ivaska, A.; Niu, L. Graphene/AuNPs/Chitosan Nanocomposites Film for Glucose Biosensing. *Biosens. Bioelectron.* **2010**, *25*, 1070–1074.
19. Bai, H.; Li, C.; Wang, X. L.; Shi, G. Q. A pH-Sensitive Graphene Oxide Composite Hydrogel. *Chem. Commun.* **2010**, *46*, 2376–2378.
20. Stankovich, S.; Dikin, D. A.; Dommett, G. H. B.; Kohlhaas, K. M.; Zimney, E. J.; Stach, E. A.; Piner, R. D.; Nguyen, S. T.; Ruoff, R. S. Graphene-Based Composite Materials. *Nature* **2006**, *442*, 282–286.
21. Kim, H.; Abdala, A. A.; Macosko, C. W. Graphene/Polymer Nanocomposites. *Macromolecules* **2010**, *43*, 6515–6530.
22. Wang, X. R.; Li, X. L.; Zhang, L.; Yoon, Y.; Weber, P. K.; Wang, H. L.; Guo, J.; Dai, H. J. N-Doping of Graphene through Electrothermal Reactions with Ammonia. *Science* **2009**, *324*, 768–771.

23. Wei, D. C.; Liu, Y. Q.; Wang, Y.; Zhang, H. L.; Huang, L. P.; Yu, G. Synthesis of N-Doped Graphene by Chemical Vapor Deposition and Its Electrical Properties. *Nano Lett.* **2009**, *9*, 1752–1758.
24. Li, X. L.; Wang, H. L.; Robinson, J. T.; Sanchez, H.; Diankov, D.; Dai, H. J. Simultaneous Nitrogen Doping and Reduction of Graphene Oxide. *J. Am. Chem. Soc.* **2009**, *131*, 15939–15944.
25. Qu, L. T.; Liu, Y.; Baek, J. B.; Dai, L. M. Nitrogen-Doped Graphene as Efficient Metal-Free Electrocatalyst for Oxygen Reduction in Fuel Cells. *ACS Nano* **2010**, *4*, 1321–1326.
26. Zhao, L.; He, R.; Rim, K. T.; Schiros, T.; Kim, K. S.; Zhou, H.; Gutierrez, C.; Chockalingam, S. P.; Arguello, C. J.; Palova, L.; *et al.* Visualizing Individual Nitrogen Dopants in Monolayer Graphene. *Science* **2011**, *333*, 999–1003.
27. Panchakarla, L. S.; Govindaraj, A.; Rao, C. N. R. Boron- and Nitrogen-Doped Carbon Nanotubes and Graphene. *Inorg. Chim. Acta* **2010**, *363*, 4163–4174.
28. Lowell, C. E. Solid Solution of Boron in Graphite. *J. Am. Ceram. Soc.* **1967**, *50*, 142–144.
29. Endo, M.; Hayashi, T.; Hong, S.-H.; Enoki, T.; Dresselhaus, M. S. Scanning Tunneling Microscope Study of Boron-Doped Highly Oriented Pyrolytic Graphite. *J. Appl. Phys.* **2001**, *90*, 5670–5674.
30. McKee, D. W. In *Chemistry and Physics of Carbon*; Thrower, P. A., Ed.; Marcel Dekker: New York, 1991; Vol. 23, p 173.
31. Kim, C.; Fujino, T.; Miyashita, K.; Hayashi, T.; Endo, M.; Dresselhaus, M. S. Microstructure and Electrochemical Properties of Boron-Doped Mesocarbon Microbeads. *J. Electrochem. Soc.* **2000**, *147*, 1257–1264.
32. Carroll, D. L.; Redlich, Ph.; Blase, X.; Charlier, J.-C.; Curran, S.; Ajayan, P. M.; Roth, S.; Ruhle, M. Effects of Nanodomain Formation on the Electronic Structure of Doped Carbon Nanotubes. *Phys. Rev. Lett.* **1998**, *81*, 2332–2335.
33. Hsu, W. K.; Firth, S.; Redlich, P.; Terrones, M.; Terrones, H.; Zhu, Y. Q.; Grobert, N.; Schilder, A.; Clark, R. J. H.; Kroto, H. W.; *et al.* Boron-Doping Effects in Carbon Nanotubes. *J. Mater. Chem.* **2000**, *10*, 1425–1429.
34. Lherbier, A.; Blase, X.; Niquet, Y.-M.; Triozon, F.; Roche, S. Charge Transport in Chemically Doped 2D Graphene. *Phys. Rev. Lett.* **2008**, *101*, 036808.
35. Martins, T. B.; Miwa, R. H.; da Silva, A. J. R.; Fazzio, A. Electronic and Transport Properties of Boron-Doped Graphene Nanoribbons. *Phys. Rev. Lett.* **2007**, *98*, 196803.
36. Elman, B. S.; Dresselhaus, M. S.; Dresselhaus, G.; Maby, E. W.; Mazurek, H. Raman Scattering from Ion-Implanted Graphite. *Phys. Rev. B* **1981**, *24*, 1027–1034.
37. Naeini, J. G.; Way, B. M.; Dahn, J. R.; Irwin, J. C. Raman Scattering from Boron-Substituted Carbon Films. *Phys. Rev. B* **1996**, *54*, 144–151.
38. Hagio, T.; Nakamizo, M.; Kobayashi, K. Studies on X-ray Diffraction and Raman Spectra of B-Doped Natural Graphite. *Carbon* **1989**, *27*, 259–263.
39. Panchakarla, L. S.; Subrahmanyam, K. S.; Saha, S. K.; Govindaraj, A.; Krishnamurthy, H. R.; Waghmare, U. V.; Rao, C. N. R. Synthesis, Structure, and Properties of Boron- and Nitrogen-Doped Graphene. *Adv. Mater.* **2009**, *21*, 4726–4730.
40. Ubbelohde, A. R.; Lewis, F. A. *Graphite and Its Crystal Compounds*; Oxford Press: London, 1960.
41. Hishiyama, Y.; Irumano, H.; Kaburagi, Y. Structure, Raman Scattering, and Transport Properties of Boron-Doped Graphite. *Phys. Rev. B* **2001**, *63*, 245406.
42. Shirasaki, T.; Derre, A.; Menetrier, M.; Tressaud, A.; Flandrois, S. Synthesis and Characterization of Boron-Substituted Carbons. *Carbon* **2000**, *38*, 1461–1467.
43. Ferrari, A. C.; Meyer, J. C.; Scardaci, V.; Casiraghi, C.; Lazzeri, M.; Mauri, F.; Piscanec, S.; Jiang, D.; Novoselov, K. S.; Roth, S.; *et al.* Raman Spectrum of Graphene and Graphene Layers. *Phys. Rev. Lett.* **2006**, *97*, 187401.
44. Dresselhaus, M. S.; Jorio, A.; Hofmann, M.; Dresselhaus, G.; Saito, R. Perspectives on Carbon Nanotubes and Graphene Raman Spectroscopy. *Nano Lett.* **2010**, *10*, 751–758.
45. Saito, R.; Gruneis, A.; Samsonidze, Ge. G.; Brar, V. W.; Dresselhaus, G.; Dresselhaus, M. S.; Jorio, A.; Cancado, L. G.; Fantini, C.; Pimenta, M. A.; *et al.* Double Resonance Raman Spectroscopy of Single-Wall Carbon Nanotubes. *New J. Phys.* **2003**, *5*, 157.1–157.15.
46. Pimenta, M. A.; Dresselhaus, G.; Dresselhaus, M. S.; Cancado, L. G.; Jorio, A.; Saito, R. Studying Disorder in Graphite-Based Systems by Raman Spectroscopy. *Phys. Chem. Chem. Phys.* **2007**, *9*, 1276–1290.
47. Lucchese, M. M.; Stavale, F.; Martins Ferreira, E. H.; Vilani, C.; Moutinho, M. V. O.; Capaz, R. B.; Achete, C. A.; Jorio, A. Quantifying Ion-Induced Defects and Raman Relaxation Length in Graphene. *Carbon* **2010**, *48*, 1592–1597.
48. Cancado, L. G.; Jorio, A.; Martins Ferreira, E. H.; Stavale, F.; Achete, C. A.; Capaz, R. B.; Moutinho, M. V. O.; Lombardo, A.; Kulmala, T. S.; Ferrari, A. C. Quantifying Defects in Graphene *via* Raman Spectroscopy at Different Excitation Energy. *Nano Lett.* **2011**, *11*, 3190–3196.
49. Cancado, L. G.; Pimenta, M. A.; Saito, R.; Jorio, A.; Ladeira, L. O.; Gruneis, A.; Souza-Filho, A. G.; Dresselhaus, G.; Dresselhaus, M. S. Stokes and Anti-Stokes Double Resonance Raman Scattering in Two-Dimensional Graphite. *Phys. Rev. B* **2002**, *66*, 035415.
50. Jiang, J.; Saito, R.; Gruneis, A.; Dresselhaus, G.; Dresselhaus, M. S. Electron−Phonon Interaction and Relaxation Time in Graphite. *Chem. Phys. Lett.* **2004**, *392*, 383–389.
51. Jiang, J.; Samsonidze, Ge. G.; Chou, S. G.; Jorio, A.; Dresselhaus, G.; Dresselhaus, M. S. Electron−Phonon Matrix Element in Single-Wall Carbon Nanotubes. *Phys. Rev. B* **2005**, *72*, 235408.
52. Attaccalite, C.; Wirtz, L.; Lazzeri, M.; Mauri, F.; Rubio, A. Doped Graphene as Tunable Electron−Phonon Coupling Material. *Nano Lett.* **2010**, *10*, 1172–1176.
53. Pisana, S.; Lazzeri, M.; Casiraghi, C.; Novoselov, K. S.; Geim, A. K.; Ferrari, A. C.; Mauri, F. Breakdown of the Adiabatic Born−Oppenheimer Approximation in Graphene. *Nat. Mater.* **2007**, *6*, 198–201.
54. Casiraghi, C. Doping Dependence of the Raman Peaks Intensity of Graphene Close to Dirac Point. *Phys. Rev. B* **2009**, *80*, 233407.
55. Huang, M.; Yan, H.; Chen, C.; Song, D.; Heinz, T. F.; Hone, J. Phonon Softening and Crystallographic Orientation of Strained Graphene studied by Raman Spectroscopy. *Proc. Natl. Acad. Sci. U.S.A.* **2009**, *106*, 7304–7038.
56. Zabel, J.; Nair, R. R.; Ott, A.; Goeogiou, T.; Geim, A. K.; Novoselov, K. S.; Casiraghi, C. Raman Spectroscopy of Graphene and Bilayer under Biaxial Strain: Bubbles and Balloons. *Nano Lett.* **2012**, *12*, 617–621.
57. Ekimov, E. A.; Sidorov, V. A.; Bauer, E. D.; Mel'nik, N. N.; Curro, N. J.; Thompson, J. D.; Stishov, S. M. Superconductivity in Diamond. *Nature* **2004**, *428*, 542–545.